

Accepted Manuscript

Geological Society, London, Special Publications

Analysis of magma flux and eruption intensity during the 2021 explosive activity at the Soufrière of St Vincent, West Indies

R. S. J. Sparks, W. P. Aspinall, J. Barclay, I. A. Renfrew, R. Contreras-Arratia & R. Stewart

DOI: <https://doi.org/10.1144/SP539-2022-286>

To access the most recent version of this article, please click the DOI URL in the line above. When citing this article please include the above DOI.

Received 14 September 2022

Revised 27 January 2023

Accepted 2 February 2023

© 2023 The Author(s). This is an Open Access article distributed under the terms of the Creative Commons Attribution 4.0 License (<http://creativecommons.org/licenses/by/4.0/>). Published by The Geological Society of London. Publishing disclaimer: www.geolsoc.org.uk/pub_ethics

Supplementary material at <https://doi.org/10.6084/m9.figshare.c.6558003>

Manuscript version: Accepted Manuscript

This is a PDF of an unedited manuscript that has been accepted for publication. The manuscript will undergo copyediting, typesetting and correction before it is published in its final form. Please note that during the production process errors may be discovered which could affect the content, and all legal disclaimers that apply to the book series pertain.

Although reasonable efforts have been made to obtain all necessary permissions from third parties to include their copyrighted content within this article, their full citation and copyright line may not be present in this Accepted Manuscript version. Before using any content from this article, please refer to the Version of Record once published for full citation and copyright details, as permissions may be required.

Analysis of magma flux and eruption intensity during the 2021 explosive activity at the Soufrière of St Vincent, West Indies

Sparks, R. S. J.¹, Aspinall, W. P.¹, Barclay, J.², Renfrew, I. A.², Contreras-Arratia, R.³ and Stewart, R.^{3,4}

¹School of Earth Sciences, University of Bristol, Bristol BS8 1RJ, UK

²School of Environmental Sciences, University of East Anglia, Norwich NR4 7TJ, UK

³Seismic Research Centre, University of the West Indies, St. Augustine, Trinidad and Tobago

⁴Montserrat Volcano Observatory, Montserrat, West Indies

Abstract

Seismic RSAM signals and eruption cloud height measurements were used to estimate peak intensities of 40 explosive events during the 8-22 April 2021 activity of the Soufrière volcano. We estimated magma supply rates and erupted volumes in each explosion, characterized uncertainty by stochastic modelling and identified four eruptive stages. Stage 1 included an intense period of 9.5 hours with 11 explosive events with peak eruption intensity between 2000 and 4000 m³/s and magma supply rate reaching 828 m³/s. 12 high intensity explosions (~4000 m³/s) occurred in Stage 2 with average magma supply rate of 251 m³/s. Stage 3 involved declining intensity, magma supply rate and lengthening repose periods between explosions. Stage 4 involved 3 much weaker explosions. The total erupted volume of magma is estimated at 38.5 x 10⁶ m³ (90% credible interval: [22.0 .. 61.9] x 10⁶ m³) consistent with independent estimates from analysis of tephra deposits and volcano subsidence sourced at ~6 km depth. The 150-fold increase in magma supply rate, from the preceding effusive phase to Stage 1 of the explosive phase, is attributed to replacement of very high viscosity degassed magma occupying the shallow conduit system with new lower viscosity volatile-rich magma from the magma chamber.

Introduction

The Soufrière of St Vincent volcano entered a major phase of explosive eruptions on 9th April 2021, following an initial phase of lava extrusion that began on 27th December 2020 (Joseph et al. 2022). At least twenty-four discrete explosive eruptions and one prolonged period of continuous but fluctuating explosive activity occurred between 9th April and 14th April 2021. A further three much weaker explosions took place on 16th, 18th and 22nd April. The explosive eruptions were documented from Real-time Seismic Amplitude Measurement (RSAM: Endo and Murray, 1991) records and from satellite observations (GOES16), which enabled cloud heights to be measured. Cloud height determinations allow the peak intensity of each explosion to be estimated. Seismic data in the form of Real-time Seismic-Amplitude Measurement (RSAM) constrain the duration of each explosion. Basic information on the explosive events is listed in Table 1.

Together with their intensities, explosion durations let us quantify cumulative erupted magma volumes, and allow variations in magma discharge rates to be estimated and tracked. In this paper we present an analysis of the RSAM and satellite observations and develop a conceptual model of the explosive phase of the eruption, taking account of other geological, geophysical and petrological observations. The study includes appraisals of the challenges entailed in interpreting proxy measurements of intensity and magma discharge rates from seismic and satellite data. These difficulties lead to significant uncertainties which are explored using stochastic uncertainty modelling principles. Our findings are compared with independent estimates of erupted volumes from analysis of tephra deposits and from ground deformation measurements. The evolution in the inferred erupted volume characteristics of the explosions is interpreted in terms of changes in the overpressure of the magma chamber and alterations to the state and dimensions of the shallow vent-conduit system.

Background

Episodic Vulcanian to sub-Plinian explosive eruptions are a common feature of many arc volcanoes (e.g. Druitt et al. 2002; Hoblitt et al. 1996; Wallace et al. 2022). Due to their transient nature such periods of episodic explosive volcanism pose problems of estimating the magma fluxes and the causes of episodic behaviour are open to several different explanations.

The period of episodic explosive eruptions at the Soufrière Volcano, St Vincent between 9th and 22nd April 2021 provides a rich dataset to address the problem of estimating eruption intensity, eruption duration and magma flux (Joseph et al. 2022; Robertson et al. this volume). The explosions were observed from the ground (Figure 1) and GOES-16 satellite monitoring as short-lived sudden onset and pulsating events. Seismic and satellite observations of plume height provide the basis for making estimates of eruption characteristics. The eruption has also been well documented in other respects, notably from studies of tephra fall out deposits (Cole et al. this volume), ground deformation (Camejo-Harry et al, this volume; Dualeh et al. 2023) and petrology (Weber et al., this volume; Frey et al, this volume).

Observations including analysis methods

Seismic Observations

The Soufrière St Vincent volcano RSAM data, recorded on seismograph station SVV (Joseph et al. 2022), show pronounced bursts of seismic activity related to tremor signals (Figure 2).

The RSAM uses 1 minute time windows with no overlap. For calculation of RSAM we removed the instrument response to compare (internally) different stations with different instruments. The seismic spectrograms depict banded tremor with fluctuating frequency content (Figure 3). The most pronounced band, containing a large range of frequencies, coincides with the initial sharp RSAM spike at 12:36 UTC on 9 April 2021, at the time of the first volcanic explosion. Indeed, the close correlation of the RSAM spikes with visible explosion clouds from the ground and appearance of rising ash clouds from satellite images (GOES-16) leads us to the conclusion that RSAM is predominantly a signature of the explosive process, although other surface or near surface processes will contribute to RSAM. Many of these bursts have sharp onsets, a pronounced maximal spike, typically lasting several minutes, and then a decline in amplitude lasting a few tens of minutes (Figure 3a). Following such events, there is usually a period of low RSAM representing a quiet period prior to the next event. However, the shapes of the RSAM signals vary (Figure 3) between a majority group that shows a very sharp onset peak followed by a slower decline (type 1) and a minority group with less accentuated, more symmetrical amplitude envelope (type 2). Type 1 with well-defined spike shapes (Figure 3b) are generally followed by a tail of declining RSAM amplitude, the waveforms of which again vary between events, ranging from those indicating smooth exponential decline to those which have a wavy, unsteady shape. The majority of type 1 RSAM events were associated with visual observations of sudden onset explosions from the ground. They have been identified with an event number assigned to observations made at the time (Table 1).

We note that a number of smaller of RSAM events do not show the same pronounced spikes (e.g., Figure 3c). Some of these were not associated with visual observations of explosions or they occurred in periods of poor visibility (e.g., with extensive cloud cover on the volcano). Thus, we have excluded any questionable RSAM disturbances from our inventory of putative explosion events. We do not know the exact cause of these RSAM perturbations but hypothesize that they may have related to surface or near-surface processes, such as landslides within the crater and conduit or simply sustained intense degassing episodes without explosions.

There was a period of more continuous but fluctuating explosive activity which lasted 9.5 hours between 18:59 (April 9th) to 04:30 (April 10th), during which we identify potential or likely individual explosive events based on the envelope shapes of RSAM amplitude spikes (Figure 3c) and on the presence of peaks of low frequency (below about 0.1 Hz) seismic energy in the corresponding spectrogram. This period is interpreted as involving explosions closely spaced in time, with some discernible RSAM event signals associated with explosive activity, emerging above the elevated seismic noise when the next impulsive explosion takes place. We have identified eleven credible explosion spikes in this 9.5 hour period and data on their duration and timing is given in Table 2. Three of these 11 spikes were initially recognised in the RSAM data, in real time at the UWI Seismic Research Centre's headquarters in Trinidad & Tobago and at the local Belmont volcano observatory (Robertson, this volume). We retained the original numbering IDs (2 to 4) to ensure our Table 1 list numbering corresponds with the official channels.

For each explosive event we measured the onset time and spike width (seismic duration) from the instrumental RSAM records; data are presented in Tables 1 and 2. Explosion (spike) durations had a mean of 13.2 minutes and ± 1 standard deviation of 5.9 minutes, with longest and shortest durations being 24 and 2.7 minutes, respectively. The explosion signals were followed by longer periods of low tremor (or coda) that occupied most of the repose

periods between explosions. Satellite images of the eruption clouds indicate that the low RSAM tremor was not associated with generation of high eruption columns. Each RSAM event duration is analysed in terms of the number of seconds elapsing from start to end of the spike trace, with uncertainties assessed using three classes to reflect the analyst's judgement of the timing measurement accuracy. The classes adopted are: ± 15 sec; ± 22.5 sec; ± 30 sec (i.e., within ± 3 standard deviations). These uncertainties are no worse than 5%, 7.5% or 10% of the measured duration of a typical RSAM spike lasting approximately 800 sec, respectively, depending on which accuracy class is ascribed to the spike measurement.

Satellite Observations

Cloud heights were estimated from satellite observations of cloud top temperatures using infra-red measurements and local in situ atmospheric temperature profiles. Data were from GOES16 thermal infra-red satellite imagery (band 13, $10.3 \mu\text{m}$) at <https://rammb-slider.cira.colostate.edu>. Plume IR brightness temperatures were taken as the minimum in the vicinity of St Vincent. The minima typically occurred 10-30 minutes after the eruption time and 20-80 km downwind, accommodating the time and distance of the ash cloud ascent. The estimated uncertainty in temperature readings is $\pm 2\text{K}$. Eruption times are given to the nearest 10 minutes. Satellite imagery during explosive activity in the 9.5 hour period between 18:59 UTC (9th April) to 04:30 UTC (10th April) showed continuous plume generation albeit with some pulsations, observations consistent with the occurrence of continuous fluctuating tremor. Data are listed in Tables 1, 2 and 3.

Brightness temperatures were translated to a height by comparing to atmospheric temperature profiles from radiosonde ascents from Grantley Adams Airport (78954 TBPB) on Barbados. Soundings are available at 12 UTC daily and are assumed to be representative of the upper troposphere atmospheric temperature over St Vincent. Inspection of meteorological re-analysis products for the upper troposphere supports this assumption. Daily radiosonde data are available at <http://weather.uwyo.edu/upperair/sounding.html>. Sounding observations have to be interpolated in height, adding a small error of around ± 0.1 km. Consequently, an uncertainty in brightness temperature of $\pm 2\text{K}$ will lead to an uncertainty in height of ± 0.3 km. There is also some uncertainty in assuming the plume is in thermal equilibrium with the atmosphere, so perhaps a conservative total uncertainty in cloud height would be ± 0.5 km. Our methodology follows that of Krueger (1982). In Table 1 these heights are listed as "Tropospheric Heights" and are the heights used in our subsequent analysis to infer discharge rates.

A complementary analysis has been done by NASA, using MISR (Multi-angle Imaging SpectroRadiometer) stereo observations at visible wavelengths (Yue et al., 2022) and CALIPSO spaceborne backscatter lidar (<https://earthobservatory.nasa.gov/images/148190/tracking-la-soufrieres-plume>). The MISR analysis indicates that the plume was dominated by non-spherical aerosol particles (likely ash) reaching up to 20 km during 10 April 2021, although much of the plume concentrated between 9 and 16 km. In Table 1, heights from the NASA analysis are listed as "Stratospheric Heights." The particles near plume top could be sulfate aerosols or small ash particles, either of which would be more transparent to infra-red than visible radiation. However, infra-red techniques generally tend to sample deeper into vertically extensive aerosol plumes (e.g., Flower and Kahn, 2020), which can explain the difference between plume heights retrieved in the visible and infra-red. In the current study, we treat the plume as concentrated in the troposphere

when presenting the analysis in terms of discharge rates and volumes, as this might skew toward the centroid of the plume.

Converting column heights to explosion intensities

The column height, H , in kilometres can be converted into eruption intensity (dense rock equivalent magma discharge rate in m^3/s) from empirical power law relationships derived from global datasets (Sparks et al. 1997; Mastin et al. 2009; Woodhouse et al. 2013). The relationship can be expressed as

$$Q = KH^n \quad (1)$$

where Q is discharge rate, K is a scaling constant and n is an empirical exponent. The above formula is derived from the analysis of global datasets with different atmospheric temperatures, initial ejecta temperatures and humidity profiles, different eruption mixture initial temperatures, latent heat generation, specific heats of ash and wind speeds which affects height through entrainment. If these parameters were known for St Vincent uncertainties in n and K could be reduced to some extent but the gain would likely be marginal and would take a lot of work to do properly so the ascribed uncertainties are going to be conservative. Initial eruption mixture temperature is a major source of uncertainty. This temperature is not known well because we do not know how much cold rock is involved for each event. Our choice of the uncertainties in n and K are guided by the scatter of data around best fit power law regressions and we comment further below on the last three weak explosions and associated plumes with low heights.

Here, values of the coefficient K and exponent n are chosen as $K = 0.51 \pm 0.08$ and $n = 4.0 \pm 0.2$. The curves generated by applying end member values of n and K bound almost all known data (Mastin et al., 2009). The formula is applied to each St Vincent event column height to estimate mean magma flux in the explosion (see Supplementary Material for more information).

Finally, application of Equation 1 is for a steady plume, but some complications are expected due to the likely unsteady and short-lived character of the explosions at the Soufrière volcano. Sparks and Wilson (1982) measured the dynamics of an explosion at St Vincent from film in 1979 and observed that the plume developed through the amalgamation of several pulses of increasing intensity over the first few minutes. The plume reached 10 km height in about 4 minutes. If an RSAM spike duration is related to explosion intensity, the shape of the RSAM spike can be interpreted as evidence of waxing intensity, passing through a peak value and then waning in amplitude. The RSAM-based durations of the events are typically only a factor of 2 or 3 times greater than the cloud ascent times but this is sufficient for Equation 1 to hold (Sparks et al. 1997). However, these complications impinge on the assessment of total mass erupted, as discussed further below.

Volumes and magma discharge rate

For each explosive event we first calculate an erupted magma volume from the product of peak intensity and spike duration. However, as discussed in the previous section, we anticipate that this will be an over-estimate because the intensity is likely to wax and wane over the duration of the event and greatest cloud height is expected to relate to peak intensity. We make a simple adjustment to reflect the unsteadiness in eruption intensity during an explosive event based on RSAM signal shape, as discussed further below. These volume results can be compared to other independent estimates of volume and discharge rate.

We remark on the interpretation of cloud height data to infer magma discharge rates. As noted in the previous section on seismic observations the discrete explosions have sharp peaks in tremor as indicated by the RSAM signals, commonly followed by exponential declining tremor. However, in explosive event 2 there is compelling evidence for significant fluctuations in tremor energy during

the event. If volcanic tremor is a proxy for discharge rate then these observations suggest large discharge rate variations across the peak. In this paper we infer that the cloud height measurements reflect peak discharge rates, so the challenge becomes how best to estimate discharge rate variations to enable erupted magma volumes to be estimated.

Detailed modelling of unsteady short-lived explosive eruptions is not yet available. Furthermore, RSAM signals of explosive events likely include energy sources that are not directly related to eruption intensity *per se*, such as simultaneous collapse of vent crater walls and other unstable or provoked surface processes. Initially, we tackled the unsteadiness of the source by noting that the shape of many RSAM spikes can be approximated as exponential growth in the waxing stage (i.e., before maximum amplitude) and an exponential decay in the waning stage (after the spike peaks). This suggests an adjustment of $(1-1/e)$ for the intensity averaged over the entire spike duration which would reduce the peak intensity estimated from the cloud height by 63%.

However, the variations and asymmetries in the amplitude shapes of different events implied this general adjustment might obscure some dynamic information contained in the event envelopes. So we investigated the areas under the recorded signal envelopes as metrics of their effective durations, relative to the simple duration-peak amplitude rectangular wave shape we had initially taken to characterize the duration of these events. On average, the spike area metrics indicated the peak intensity from cloud height would be reduced by $40\% \pm 10\%$ (1 s.d.), rather than 63% as per the basic exponential adjustment.

In the analysis which follows, we therefore determine re-scaled effective explosion intensities using our RSAM spike waveform area measurement adjustments, event-by-event, and estimate the volume erupted in each explosion as the product of duration and the corresponding power law-scaled peak intensity.

Finally, we assess the magma supply rate from the calculated volume associated with each explosion divided by the repose period following the preceding explosion. Here, supply rate is defined as the flux rate from the deeper magma system, located at about 6 km depth from ground deformation observations (Joseph et al. 2022; Camejo-Harry et al., this volume). We expect this flux to be highly unsteady because an explosion will evacuate the upper parts of the conduit of magma, which will subsequently refill prior to the next explosion. The consequence of this cycling is that there will be large variations in driving pressure and flow rate, and thus our estimation for an individual explosion is a supply rate which is averaged over that changeable magma flux.

There is one important limitation to our estimates of magma supply rate and total erupted magma volume. Our estimates are based on explosive intensities for the high eruption columns, but do not take account of magma erupted to form pyroclastic density currents from column collapse. Thus estimates of erupted magma volume and of magma supply rate in Stages 2 and 3, when the pyroclastic density currents were generated, are underestimates. However, we can obtain an approximate evaluation of this underestimate from the results presented by Cole et al. (this volume). Cole et al. estimate a total bulk volume of tephra of $119 \times 10^6 \text{ m}^3$ ($\pm 24 \times 10^6 \text{ m}^3$) and a bulk volume of pyroclastic density currents of $17 \times 10^6 \text{ m}^3$ ($\pm 3.5 \times 10^6$). Thus the underestimate is evaluated at between 10% and 20%.

Stochastic modelling and uncertainty

We used the stochastic analysis software UNINET to apply Eq. 1 to each explosion case, allowing us to incorporate approximate uncertainties associated with the empiricism embedded in this equation (noted above) while, at the same time, not neglecting likely uncertainties related to the observational data. The UNINET program (<https://lighttwist-software.com/uninet/>) is a standalone uncertainty analysis software package with a focus on dependence modelling for high dimensional

statistical or probability distributions (Hanea et al. 2010). UNINET has been widely deployed in the earth and environmental sciences (e.g. Christopherson et al. 2018; Cooke et al. 2018; Bamber et al. 2022).

In this way, we can estimate the peak intensity of each explosive event from satellite cloud height observations, the magma volume discharge for each explosive event and an indicative magma supply rate (from the magma volume of an explosive event divided by the preceding repose period). Further details of the stochastic uncertainty model are provided in Supplementary Material.

Including attendant uncertainties in these calculations permits us to express our analysis results fully in terms of defined uncertainty quantiles (e.g., mean and standard deviation on the mean; 5th percentile, median and 95th percentile; or 90% credible interval CI), and not simply produce single 'best estimate' point values. We note that the uncertainties that characterize the measurements of cloud height and conversion to intensities are a mixture of epistemic and aleatory uncertainties and that they are not straightforward to de-aggregate and analyse separately.

Results

Using our preferred RSAM waveform area adjusted duration and intensity estimations, results for our stochastic calculations for the St Vincent explosive events are reported in the accompanying Table 3. The vent elevation in the crater of the Soufrière is 0.7 km a.s.l. leading to an adjustment to the column height data in Tables 1 and 2 when applying Equation 1 in the UNINET model.

Intensity, magma discharge rate and volumes

We present the data in time series plots: cumulative magma volume (Figure 4); intensity of individual explosive events (Figure 5); magma supply (i.e., event volume divided by preceding repose time (Figure 6); and repose periods (Figures 7 and 8). The time series for volume (Figure 4) visualizes the evidence for major changes in the activity. We identify three Stages of activity up to 14th April and a fourth Stage comprising the last three weak explosions 30, 31 and 32 (Table 1). We have excluded the fourth Stage on the cumulative volume plot (Figure 4), intensity time series plot (Figure 5) and magma discharge rate plot (Figure 6) as the contributions of these late-stage events are very small.

In Figure 4, we plot two variants of the uncertainty spreads associated with the cumulative DRE (Dense Rock Equivalent) volume estimates, arising from alternative ways of applying Equation 1 to the explosions data. In one form of analysis, at each sampling iteration a random value for coefficient K and one for exponent n are drawn from their uncertainty distributions (see Supplementary Material) and applied to all explosions. In essence, this approach says that while we are not sure about the 'right' values of K , n to use, i.e., epistemic uncertainty, we assume there is such a pair and apply them to all explosions, simultaneously. Each individual run thus has fixed values of K and n for every explosion. We carried out 50,000 runs each with fixed K and n with values drawn for each randomly from the probability distributions of K and n . The resulting 5th and 95th percentiles are labelled "fixed K , n all explosions" in Figure 4.

However, as discussed in relation to the basis for Equation 1 above, there are physical reasons to believe K , n can vary from one explosion to another (i.e., some aleatory uncertainty will exist). Thus, in a second analysis, separate random samples of K , n are drawn for and applied to each explosion independently, i.e., these multiple values of K , n are uncorrelated. We carried out 50,000 runs with completely randomised K , n for each and every explosion for each model run. The resulting uncertainty percentiles are labelled "independent K , n each explosions".

With respect to both sets calculations using Equation 1 for individual explosions, the differences in estimated event uncertainties are small. However, these small effects become compounded as the explosion volumes are accumulated as the eruption progresses (Figure 4). Assuming K , n are fully correlated results in much wider cumulative volume uncertainty spreads when compared with the alternative, uncorrelated assumption. For the present eruption, best estimates of the uncertainty ranges likely fall between these two end member assumptions. It can be argued that values of K , n are probably much less varied than the global data imply yet do vary from one explosion to the next with some degree of correlation, i.e., a process 'memory' is involved. For the case of the 2021 St Vincent explosions, exploration of this issue and how to constrain uncertainties appropriately may be amenable to later, detailed modelling analysis.

The first Stage starts with an initial explosive event 1 at 12:36 UTC 09 April 2021 and then, just over six hours later, the activity escalates into a succession of 11 closely spaced explosive events over 9.5 hours, starting at 18:59 UTC 09 April and finishing at 04:30 UTC 10 April. During this period, volcanic tremor (Figure 2) is continuous, and the volcanic plume is observed to have been present continuously above St Vincent from satellite images. Subject to the challenges of measuring individual RSAM spikes in this period of elevated seismic tremor, eruption intensity climbs to a peak ($3.9 \times 10^3 \text{ m}^3/\text{s}$) with event 4 at 00:11 UTC 10 April 2021 (Figure 5).

Figure 6 reveals that the magma supply rate had already peaked in this Stage of the eruption, reaching a maximum of nearly $830 \text{ m}^3/\text{s}$ at event P09 in the 9.5 hour sequence (i.e., at 00:32 UTC 10 April, red markers to about 12 hours elapsed from first explosion).

Thereafter, the magma supply rate in Stage 1 dropped substantially, with one reversal, to only $30 \text{ m}^3/\text{s}$ by event 6 at 07:24 10 April, after over 18 hours had elapsed (Figure 6).

To accord with other, visual observations, therefore we define the end of this first Stage as the explosive event 6 at 07:24 UTC 10 April, which correlates with tephra fall deposit U1 during this stage (Cole et al; this volume). Satellite images (*ICEYE* and *Capella*) show that a big new explosion crater had formed before 10:00 UTC 10 April, resulting in the destruction of the recently emplaced 2020-21 lava dome and of much of the 1979 lava dome (Joseph et al. 2022). A satellite image provided by Raphael Grandin shows this as a new explosion vent measured 650 m wide and was at least 100 m deep. Thus, we infer Stage 1 is associated with this explosion crater formation and we note that its dimensions remained little changed after this time. Repose periods between explosions reached a minimum during Stage 1 (Figure 8).

The second Stage starts abruptly at 09:35 UTC 10 April 2021 and consists of twelve explosive events, occurring in the interval depicted in Figures 5 and 6 between 20 - 44 hours elapsed time since the first explosion. During Stage 2, explosion intensities are uniformly at high levels, about $4 \times 10^3 \text{ m}^3/\text{s}$ (Figure 5) and corresponding time-averaged magma supply rates are also generally sustained high, typically about $200 - 400 \text{ m}^3/\text{s}$ (Figure 6). Note that the magma supply rate may be underestimated by 10-20% in Stage 2 because pyroclastic density current deposit volumes are not included. Repose periods are short (~ 0.8 to 2.5 hours), but sufficiently long that the explosive events are discrete, both from satellite images and in RSAM (Figure 3b). We judge the end of Stage 2 at 04:59 UTC 11th April when nearly 41 hours had elapsed since the initial explosion and the magma supply rate was in decline thereafter (Figure 6).

A third Stage shows decreasing intensity of explosive events from 07:55 UTC 11 April (Figure 5: green markers), and decelerating magma supply discharge, reflecting, in part, growing

repose intervals between explosions (Figures 7 and 8). This Stage is judged to have ended after 15:31 UTC 14th April 2021, when 123 hours had elapsed since the first explosion of the eruption. We then infer that the volcano enters a fourth and final Stage characterized by three much weaker explosions until 22nd April 2021, with much longer inter-event intervals and with volume erupted per event more than two orders of magnitude less than the previous explosive events (Table 4). Corresponding magma supply rates were very low $<0.1 \text{ m}^3/\text{s}$, but these values may not be meaningful, as discussed below.

Taking the three Stages from 9th to 14th April 2021 overall, the adjusted RSAM durations fall between 2.7 and 24 minutes (Table 1) and explosive eruptions are characterized by column heights in the range 10.0 to 16.2 km. Using Equation 1, the equivalent mean intensities, across the three stages, range from 540 to 4160 m^3/s (Figure 5). The average of the mean intensities of the explosions is 3050 m^3/s with standard deviation on the mean $\pm 940 \text{ m}^3/\text{s}$. The stochastic uncertainty analysis yields an average 5th percentile intensity value which is about 50% of this average mean value and a 95th percentile that is 73% greater.

Mean erupted volumes per explosion vary between 0.1 and $2.46 \times 10^6 \text{ m}^3$ with an average volume per event of $1.02 \times 10^6 \text{ m}^3$. Stochastic uncertainty analysis yields a 5th percentile that is 50% of the mean and a 95th percentile 73% greater than the mean (because there is a linear relationship with the calculations for intensities, presented above, these estimates are as expected but serve to validate the calculations).

The erupted volume (mean value) for Stage 1 is calculated as $10.0 \times 10^6 \text{ m}^3$ with 90% credible interval CI: $[7.4 \dots 13.3] \times 10^6 \text{ m}^3$. Stage 2 mean erupted volume amounts to $18.3 \times 10^6 \text{ m}^3$ CI: $[9.1 \dots 31.5] \times 10^6 \text{ m}^3$, while Stage 3 explosions provide a mean of $10.2 \times 10^6 \text{ m}^3$ CI: $[5.1 \dots 17.4] \times 10^6 \text{ m}^3$. Thus, by the end of Stage 3, the mean estimated total volume erupted is $38.5 \pm 2.7 \times 10^6 \text{ m}^3$ CI: $[22.0 \dots 61.9] \times 10^6 \text{ m}^3$. Note that credible interval here is defined by the 5th and 95th percentiles. Note that the pyroclastic density currents discharged in Stages 2 and 3 and are not included in these calculations.

In Figure 6, the mean magma supply discharge in Stage 1 averages $257 \text{ m}^3/\text{s}$ ($\pm 247 \text{ m}^3/\text{s}$ 1sd). While the average supply discharge in Stage 2 remains approximately the same ($258 \text{ m}^3/\text{s}$), the fluctuations are much smaller ($\pm 86 \text{ m}^3/\text{s}$ 1sd). In Stage 3, this supply declines to $81 \text{ m}^3/\text{s}$ ($\pm 47 \text{ m}^3/\text{s}$ 1sd). The three events after 14th April 2021 give apparent flux rates of only about $25 \text{ m}^3/\text{s}$ which is exceedingly low and suggests that these weak Vulcanian events did not involve conduit filling and emptying cycles, but represented a form of minor, residual explosive activity.

Comparison with tephra volumes

Our erupted magma volumes can be compared with alternative methods. Cole et al. (this volume) divided the tephra fall deposits formed between 9th and 22nd April into seven stratigraphic Units. By combining field characteristics of the different Units, satellite observations and visual observations from the ground, they have linked the main stratigraphic Units to dates and events. They estimate the bulk volumes of tephra fall deposits during the eruption using an expert elicitation procedure to combine the judgements of several experts who independently drew isopach maps from field thickness data for each of the tephra Units U1, U2, U3 and U4-7 and also for the total deposit thickness. A conversion factor of 0.6 was used to convert from bulk to dense rock equivalent (DRE) volume (P. Cole, personal communication).

Cole et al.'s estimates yield a DRE volume of 39.2 million m^3 CI: $[22.3 \dots 61.4] \times 10^6 \text{ m}^3$ from the summed individual isopach maps and 31.6 million m^3 CI: $[15.4 \dots 58.5] \times 10^6 \text{ m}^3$ from the

total deposits isopach map. These central estimate results are in apparently very good agreement with our estimate of $38.5 \times 10^6 \text{ m}^3$ CI: $[22.0 \text{ .. } 61.9] \times 10^6 \text{ m}^3$. However, this agreement needs some circumspection since not all the uncertainties are fully included in either of the estimates. The estimate of Cole et al. (this volume) is based on tephra thickness maps and uncertainty in the proportions of lithic clasts is not included in the conversion to magma volumes. In addition the volume estimate does not include tephra deposited within the crater and magma erupted as pyroclastic density currents. Thick tephra cones formed around the newly formed crater and Cole et al. (this volume) estimate that the DRE volume of these very proximal tephra deposits in the crater is approximately $26 \times 10^6 \text{ m}^3$ ($\pm 4 \times 10^6 \text{ m}^3$). An unknown proportion of the heat from the proximal tephra and pyroclastic density current should have contributed to the buoyancy of the tephra plume. There is also uncertainty on ash and tephra deposition related to meteorological influences during the eruptive events (see Poulidis et al. 2019). We thus prefer to highlight that the volume estimates are consistent with one another and overlap in uncertainty ranges. Table 4 reports our corresponding erupted DRE volume estimates for the main stratigraphic units identified by Cole et al (this volume). The agreement with the individual units and our volume results for the same time interval is less good than for the total volumes but nonetheless well within the uncertainty limits of both independent estimation methods. The volume difference between U4-U7 may reflect that the isopach map is more poorly constrained during the later period (Cole et al. this volume).

Comparison with deformation data

Ground deformation prior to and during the eruption provide approximate estimates of magma volumes involved (Camejo-Harry et al., this volume). Between July and December 2020 an inflation with an estimated volume of 29 million m^3 at a depth of 18 km was observed. During the first three days of the explosive eruption, corresponding to Stages 1 and 2 and the first part of Stage 3, a major subsidence was observed at an inferred depth of 6 km with a volume change of 50 million m^3 . This volume estimate falls just within the 90% credible interval of the corresponding estimate from our RSAM measurements: i.e., $38.5 \times 10^6 \text{ m}^3$ CI: $[22.0 \text{ .. } 61.9] \times 10^6 \text{ m}^3$. However, this comparison with explosion volumes does not take account of the additional magma associated with pyroclastic density current deposits (PDC) and as very proximal tephra fall deposits within the crater whose heat contribution to the plumes is not known.

Comparison with volume estimates from seismic data

Latchman and Aspinall (this volume) applied the seismic moment method to estimate internal volume change in the magmatic system over the entire eruption from July 2020 to the end. The approach is based on log-log regression of intruded magma volume as a function of cumulative seismic moment release, including representative uncertainties in each (Meyer et al. (2021). Their overall estimate is $68 \pm 14 \times 10^6 \text{ m}^3$ DRE magma, which is close to the estimate of $71 \pm 14 \times 10^6 \text{ m}^3$ DRE by Cole et al. (this volume). Our estimate of $38.5 \times 10^6 \text{ m}^3$ CI: $[22.0 \text{ .. } 61.9] \times 10^6 \text{ m}^3$ is consistent with both results, noting that it does not take account of the pyroclastic density current deposits and some poorly known fraction of the proximal crater fill deposits

Finally, we also explored relationships of eruption magma volume, duration and cloud height with the preceding and following repose periods and found no convincing systematic correlations.

Discussion

The initial extrusive phase of the eruption involved steady extrusion of residual degassed magma residing at shallow level within the 1979 dome interior and underlying upper conduit system (Stinton et al., this volume). The almost constant extrusion rate observed in this period (27th December 2020 to 6th April 2021; Joseph et al., 2022) is taken to represent an approximately constant overpressure related to the ascent of volatile fresh magma from a magma chamber residing at a depth of several kilometres. Much of the viscous resistance to magma flow during the extrusive phase is attributed to pushing out a degassed plug of very viscous magma that occupied the upper parts of the conduit (Stinton et al., this volume). Prior to the onset of explosive activity VT swarms were observed on 23rd March and 5th April, and banded tremor was observed on 5th April (Joseph et al. 2022). In the last 1 to 2 days (7th and 8th April) a marked increase in extrusion rate was observed (Dualeh et al. 2023) with incandescence and bulging of the new lava in the source region (Joseph et al. 2023). These precursors to the onset of the explosive phase are inferred to represent a surge in magma ascent caused by much less viscous gas-rich magma reaching close to the surface, which then led into the explosive phase.

Geophysical and petrological observations place the magma chamber at a depth of 6 to 8 km (Camejo-Harry et al., Frey et al. and Weber et al. this volume). These two parts of the system interact through controlling the driving pressure for flow. We allude to a model for vent evolution developed for kimberlite pipe evolution (Sparks et al., 2006, Sparks 2013) that we consider to be a generic model for how evolution of conduit-vent systems control eruption rates and eruptive styles. Early on in the process, there is a crater formation regime during which explosive flows are over-pressured on exit. Eventually the crater is wide enough that the explosive flows reach atmospheric pressure at or within the developing crater. At this second stage pyroclastic ejecta can start to infill the crater-vent system and the explosive flows start to interact with the infills. Readers are referred to Figure 8 and 11 in Sparks (2013) for a fuller description of the evolution of vent-conduit systems and the associated flow dynamics.

Following the onset of explosive activity on 9th April 2021, the new dome and much of the 1979 dome was destroyed forming new nested craters within the main crater of the volcano. This represents the early regime of vent-conduit evolution and the new explosion crater was established by 09:35 UTC on 10th April. This period of crater formation coincides with an increasing intensity of Stage 1 explosions, inferred from our proxy RSAM measurements, and suggests that significant explosive energy was expended in crater formation. The incorporation of abundant cold lithic material into the eruption columns, as indicated from studies of the equivalent tephra fall deposits (Cole et al., this volume), would have reduced the column temperature and height. As the material around the developing cratering was cleared away, the explosive flows could intensify as they exited through the wider and deeper crater. After a hiatus of a few hours, Stage 2 began with the high repetitive intensity explosive activity.

We interpret Stages 1 to 2 as cycles of evacuation of volatile-rich magma from the conduit during each explosive eruption (Latchman and Aspinall, this volume; Weber et al. this volume) followed by rapid magma ascent to refill the conduit prior to the next explosion. Magma ascent was too rapid to allow significant volatile loss in the rising magma and so an overpressure for explosive failure was crossed at the front of each ascending magma surge. Models of diffusive mass transfer of volatiles during magma ascent and show that episodic explosive eruptions can be explained by disequilibrium degassing (Mason et al.; La Spina et al. 2017). At the same time, removal of magma from the chamber led to reduction in

chamber pressure and consequent large subsidence at a depth of about 6 km (Camejo-Harry et al., this volume).

Stage 3 involved a declining intensity in the eruption. We invoke three factors that lead to this decline. First the rapid decompression of the magma chamber in Stages 1 and 2 decreased the pressure gradient driving the explosive flows, so magma ascent rates decreased. Declining conduit recharge enabled increasing gas loss during magma ascent. The apparent emergence of LP seismicity in Stage 3 (Latchman and Aspinall, this volume), which may have been obscured previously by the high amplitude tremor, can be attributed to the initiation of gas loss during ascent. Gas loss during ascent increases the density of the ascending magma column and so increases magmastatic pressures which further reduce pressure gradients driving the flows. This feedback mechanism leads eventually to either a transition to effusive eruption or leads to the eruption stopping. Empirical evidence concerning transition between explosive and effusive eruptions for silicic and intermediate magmas indicates that the transition is at around 10-20 m³/s (Sparks 1997). The decrease of recharge rate to about 17 - 25 m³/s after the end of Stage 3 on 14th April 2021 (Figure 6) is consistent with this transition having been reached.

A third factor concerns the infilling of the conduit with ejecta as eruption intensity wanes. Explosive flows must interact with the vent-conduit system fill and so some of the ejecta is either trapped in the vent or is erupted as pyroclastic materials and does not contribute to form the high eruption columns. This is also a feedback mechanism that leads into waning pressure gradients and eventually to an eruption moving into an effusive phase or stopping. The onset of explosive activity led to a rapid decompression of the chamber at depth. Rapid deflation is seen in surface deformation data recorded on the continuous GPS network on 9th April (Joseph et al., 2022). Using a Mogi point source model (Camejo-Harry et al., this volume), a volume change of $\sim 50 \times 10^6 \text{ m}^3$ was calculated at a depth of about 6 km between 9th and 22nd April 2021. This volume change is just above the 90% credible interval uncertainties of the erupted magma volumes enumerated by our preferred approach (i.e., $38.5 \times 10^6 \text{ m}^3$ CI: $[22.0 \text{ .. } 61.9] \times 10^6 \text{ m}^3$) and by study of the tephra deposits. Our approach is likely to be a minimum since juvenile material erupted as pyroclastic density currents and very proximal fall out are not taken into account.

The study of tephra deposits (Cole et al. this volume) indicates a DRE volume (including pyroclastic density currents and very proximal fall out) of $71.4 \pm 14 \times 10^6 \text{ m}^3$, but this is a maximum estimate as some of the volume will be accidental lithics rather than juvenile magma. The volume change from surface deformation modelling is expected to be a minimum since volume loss by eruption may be partly compensated by either recharge of the magma chamber or decompression-induced volatile exsolution in the chamber. Thus, there is nice harmony between these three independent assessments.

The transition from effusive to explosive eruption at the Soufrière was rapid and involved large change in magma ascent dynamics. During the early lava extrusion, magma supply rate from the chamber into the conduit system at about 1.2 m³/s (Stinton et al., this volume) was sufficiently slow for chamber volume to remain constant and overpressures to be maintained. Magma supply rate reached 251 and at least 258 m³/s in Stages 1 and 2 of the explosive phase, approximately 200 times greater than in the effusive phase, while transient flow rates during explosive events reached over 4000 m³/s, approximately 3300 times greater than in the effusive phase.

These changes can be explained by two main factors. First by a rapid change in magma viscosity with high viscosity degassed magma being pushed out by low viscosity volatile-rich and somewhat hotter fresh magma. Stinton et al., (this volume) estimated a viscosity decrease of about order four orders of magnitude over the transition. Prior to the onset of explosive activity, they infer a near surface constriction combined with very high viscosity ($\sim 10^{11}$ Pa s) degassed resulted in slow steady effusion. The early explosions of low viscosity ($\sim 10^7$ Pa s) volatile-rich magma destroyed this constriction to create the new crater and excavate a deeper conduit through which the volatile-rich magma could easily flow. The reduction in magma supply rate during Stage 3 suggests declining overpressure in the chamber augmented by the two feedback mechanisms associated with gas loss during magma ascent and evolution of the vent-conduit system. As the supply rate waned, the vent-conduit system started to refill with rock debris and tephra, further suppressing magma flow.

Conclusions

We have used seismic data in the form of RSAM signals and satellite data to measure eruption cloud heights to estimate the peak intensity of 40 explosive events in the explosive phase of the 2020-21 eruption of the Soufrière, St Vincent. These estimates can then be used as proxies to estimate magma supply and volume of magma erupted. There are some large epistemic and aleatory uncertainties associated with these estimates which we have characterized by applying a stochastic uncertainty modelling approach.

The time series of intensities, magma supply rates and volumes indicated four stages in the explosive phase of the eruptions between 9th and 22nd April 2021. Following an opening explosion at 12:30 UTC 9th April in Stage 1 an intense period of 9.5 hours of at least 11 explosive events began at 09:59 UTC 9th April. Peak eruption intensity was mostly between 2000 and 4000 m³/s. Magma supply rate peaked at about 828 m³/s midway through the 9.5 hours episode and there followed three discrete explosions with lower magma supply rates. Stage 2 started at 09:35 UTC on 10th April and involved several closely spaced explosions with similar high intensity (~ 4000 m³/s) at the same high magma supply rate, averaging 258 m³/s. Stage 2 ended following the explosion at 04:59 UTC 11th April. Stage 3 involved declining intensity, magma supply rate and lengthening repose periods between explosions. Stage 3 ended 15:31 UTC 14th April 2021. Stage 4 involved three much weaker explosions on 16th, 18th and 22nd April 2021.

The total volume of magma erupted in the explosive phase, estimated using our preferred method, is 38.5×10^6 m³ CI: [22.0 .. 61.9] $\times 10^6$ m³. For the reasons explained above, our application of fixed values for K , n in Equation 1 likely produce inflated credible intervals around the mean erupted volume results. Nevertheless, our central estimate of total DRE volume erupted in all the explosions is similar to independent estimates derived from analysis of isopach maps of the tephra fall deposits. The estimates of Cole et al. (this volume) yield a DRE volume of 39.2 million m³ CI: [22.3 .. 61.4] $\times 10^6$ m³ from the summed individual isopach maps and 31.6 million m³ CI: [15.4 .. 58.5] $\times 10^6$ m³ from the total deposits isopach map. Our estimate is also compatible with the estimate of 50×10^6 m³ of subsidence from a magma source at 6 km depth (Camejo-Harry et al. this volume).

The large change in magma supply rate between the preceding effusive eruption and the explosive eruption is attributed to the replacement of degassed magma occupying the shallow conduit system with new volatile-rich magma from a magma chamber at about 6 km depth. Arrival of much lower viscosity, new magma and the destruction of the near

surface main crater floor of the volcano, to form an explosion crater, led to the transition and an increase in magma supply rate by approximately 200 times.

Acknowledgements

The authors acknowledge support and comments on earlier versions of the paper by Paul Cole, Michal Camejo-Harry and Richie Robertson. Alvaro Aravena and an anonymous reviewer are thanked for the comments which improved the manuscript and its presentation. We thank Ralph Kahn at NASA for his thoughts on satellite-derived plume heights.

ACCEPTED MANUSCRIPT

References

- Bamber, J.L., Oppenheimer, M., Kopp, R.E., Aspinall, W. P. and Cooke, R. M. 2022. Ice sheet and climate processes driving the uncertainty in projections of future sea level rise: Findings from a structured expert judgement approach. *Earth's Future* DOI: 10.1029/2022ef002772
- Camejo-Harry, M., Pascal, K., Euillades, P., Grandin, R., Hamling, I., Euillades L., Contreras-Arratia, R., Latchman, J.L., Lynch, L., Ryan, G. and Jo, M. Monitoring volcano deformation at La Soufrière, St. Vincent during the 2020-21 eruption with insights into its magma plumbing system architecture. (This volume).
- Christophersen, A., Deligne, N.I., Hanea, A. M., Chardot, L., Fournier, N. and Aspinall, W.P. 2018. Bayesian Network Modeling and Expert Elicitation for Probabilistic Eruption Forecasting: Pilot Study for Whakaari/White Island, New Zealand. *Frontiers in Earth Science* 6(211) doi: 10.3389/feart.2018.00211
- Cooke, R.M. and Wielicki, B. (2018). Probabilistic reasoning about measurements of equilibrium climate sensitivity: combining disparate lines of evidence, *Climatic Change*, 151(3), 541-554. doi.org/10.1007/s10584-018-2315-y
- Cole, P.D. Barclay J., Robertson, R.E.A., Mitchell, S., Davies, B.V., Constantinescu, R., Sparks, R.S.J., Aspinall, W.P. and Stinton, A. Explosive sequence of La Soufrière St Vincent April 2021: insights into drivers and consequences via eruptive products. (This volume).
- Druitt, T.H., Young, S.R., Baptie, B., Bonadonna, C., Calder, E.S., Clarke, A.B., Cole, P.D. Harford, C.L., Herd, R.A., Luckett, R., Ryan, G. and Voight, B. (2002). Episodes of cyclic Vulcanian explosive activity with fountain collapse at Soufriere Hills Volcano, Montserrat. *Geological Society of London Memoir* 21, 281-306.
- Dualeh, E.W., Ebmeier, S.K., Wright, T.J., Poland, M.P., Grandin, R., Stinton, A.J., Camejo-Harry, M., Esse, B. and Burton, M. (2023). Rapid pre-explosion increase in dome extrusion rate at La Soufriere, St Vincent quantified from synthetic aperture radar backscatter. *Earth and Planetary Science Letters* 603: 117980.
- Endo, E.T. and Murray, T. (1991) Real-time seismic amplitude measurement (RSAM): a volcano monitoring and prediction tool. *Bulletin of Volcanology*, 53, 533–545. <https://doi.org/10.1007/BF00298154>
- Flower, V.J.B. and Kahn, R.A. 2020. The regional volcanology of Kamchatka, based on multi-Sensor satellite observations. *Remote Sensing Environment* 237. doi:10.1016/j.rse.2019.111585.
- Frey, H.M., Manon, M.R., Walters, S., Barclay, J., Davies, B.V., Christopher, T.E. and Joseph, E.P. Petrology of the explosive deposits from the April 2021 eruption of La Soufrière volcano, St Vincent: a time-series analysis of microlites. (This volume).
- Joseph, E.P., Camejo, M., Christopher, T., Contreras-Arratia, R., Edwards, S., Graham, O., Johnson, M., Juman, A., Latchman, J.L., Lynch, L., Miller, V.L., Papadopoulos, I., Pascal, K., Robertson, R., Ryan, G.A., Stinton, A., Grandin, R., Hamling, I., Jo, M-J., Barclay, J., Cole, P., Davies, B.V. and Sparks, R.S.J. 2020. The 2020 – 2021 eruption of La Soufrière volcano, St. Vincent: Monitoring and Scientific Response. *Nature Communications* 13: 4129. <https://doi.org/10.1038/s41467-022-31901-4>

- Krueger, A.F. 1982. Geostationary satellite observations of the April 1979 Soufriere eruptions. *Science* 216(4550), 1108-1109.
- Hanea, A.M. et al. (2010) Mining and visualising ordinal data with non-parametric continuous BBNs. *Comp Stats Data Analysis* 54, 668-687.
- Hoblitt, R.P., Wolfe, E.W., Scott, W.E., Couchman, M.R., Pallister, J.S. and Javier, D. 1996. The Preclimactic Eruptions of Mount Pinatubo, June 1991. In *"Fire and Mud: Eruptions and Lahars of Mount Pinatubo, Philippines"* (Edited by Newhall, C.G. and Punongbayan, R.S.) University of Washington Press: Seattle, WA, USA, 457–511.
- La Spina, G., de Vitturi, M. and Clarke, A.B. 2017. Transient numerical model of magma ascent dynamics: application to the explosive eruptions at the Soufrière Hills Volcano. *Journal of Volcanology and Geothermal Research* 336, 118–139.
- Latchman, J.L. and Aspinall, W.P. La Soufrière volcano, St. Vincent, eruption 2020-2021: assessing unrest and eruptive states from limited volcano-seismic data. (This volume).
- Mason, R.M., Starostin, A.B., Melnik, O. and Sparks, R.S.J. 2006. From Vulcanian explosions to sustained explosive eruptions: the role of diffusive mass transfer in conduit flow dynamics. *Journal of Volcanology and Geothermal Research* 153, 146-165.
- Mastin, L. G., et al. 2009. A multidisciplinary effort to assign realistic source parameters to models of volcanic ash-cloud transport and dispersion during eruptions, *Journal of Volcanology & Geothermal Research* 186(1–2), 10–21.
- Meyer, K., Biggs, J. and Aspinall, W. 2021. A Bayesian reassessment of the relationship between seismic moment and magma intrusion volume during volcanic unrest. *Journal of Volcanology and Geothermal Research* 419:107375: 1-10. Doi: 10.1016/j.jvolgeores.2021.107375
- Poulidis, A. P., Phillips, J.C., Renfrew, I. A., Barclay, J., Hogg, A., Jenkins, S., Pyle, D. and Robertson, R. 2018. Meteorological controls on local and regional volcanic ash dispersal, *Scientific Reports*, 8:6873, doi: 10.1038/s41598-018-24651-1
- Robertson, R.A.E. An overview of the eruption of La Soufriere Volcano, St. Vincent 2020 to 2021. (This volume)
- Sparks, R.S.J. 1997. Causes and consequences of pressurization in lava dome eruptions. *Earth and Planetary Science Letters* 150, 177-189.
- Sparks R.S.J. 2013. Kimberlite Volcanism. *Annual Review of Earth and Planetary Sciences*, 41, 97-528, 2013.
- Sparks, R.S.J. and Wilson, L. 1982. Explosive volcanic eruptions V: Observations of plume dynamics during the 1979 Soufriere eruption, St Vincent. *Geophysical Journal of the Royal Astronomical Society* 69, 551-570, 1982.
- Sparks, R.S.J., Bursik, M.I., Carey, S.N., Gilbert, J.S., Glaze, L., Sigurdsson, H. and Woods, A.W. 1997. *Volcanic Plumes*. John Wiley and sons pp. 557.
- Sparks, R.S.J., Baker, L., Brown, R.J., Field, M., Schumacher, J., Stripp, G. and Walters, A. L. Dynamics of Kimberlite Volcanism. 2006. *Journal of Volcanology and Geothermal Research* 155, 18-48, 2006.

Stinton, A., Sparks, R.S.J. and Huppert, H.E. Analysis of magma rheology from lava spreading and explosive activity during the 2020-2021 eruption of the Soufrière St Vincent with implications for eruption dynamics. (This volume).

Wallace, P., Lamb O.D., de Angelis, S., Kendrick J.E., Horby, J.A., Diaz-Moreno, A., Gonzalez, P.J., von Aulock, F.W., Lamur, A., Utley, J.E.P, Rietbrock, A., Chigna, G. and Lavallee, Y. 2020. Integrated constraints on explosive eruption intensification at Santiaguito dome complex, Guatemala. *Earth and Planetary Science Letters* 536, 116139.

Weber, G., Blundy, J., Barclay, J., Pyle, D.M., Cole, P., Frey, H., Manon, M., Davies, B.V. and Cashman, K.V. Petrology of the 2020-21 effusive to explosive eruption of La Soufrière volcano, St Vincent: Insights into plumbing system architecture and magma assembly mechanism. (This volume)

Woodhouse, M., Hogg, A.J., Phillips, J.C. and Sparks R.S.J. 2013. Interactions between volcanic plumes and wind during the 2010 Eyjafjallajökull eruption. *Journal of Geophysical Research Solid Earth* 118, 92-109.

Yue, J., Miller, S.D., Straka, W., Noh, Y-J., Chou, M-Y., Kahn, R.A. and Flower, V.J.B., 2022. La Soufriere volcanic eruptions launched gravity waves into space. *Geophysical Research Letters*. 49, doi:10.1029/2022GL09.

ACCEPTED MANUSCRIPT

Figure Captions

Figure 1. Images of explosion at 6.28 am morning of 13th April 2021 (Table 1: event 27 at 10.23 UTC).

Figure 2. Vertical seismograph waveform at station SVV with RSAM (see text) at the same station from 00:00 8 April 2021 to 00:00 23 April 2021; plotted as non-overlapping 1min time windows. Prominent spikes correspond to 40 identified volcanic explosive events (see Tables 1 and 2 for times, durations, column heights, etc.). Time is UTC and time label links to tick point above mid-point of label.

Figure 3. Examples of explosion seismic waveforms, RSAM signals and spectrograms. (a) Series of eight explosions between 20:00 10 April 2021 and 12:00 12 April showing sharp onsets to RSAM signals (middle panel) and exponential decays; note diagnostic low frequency energy (<0.1 Hz) in spectrograms. (b) Explosion at 10:23 13 April showing extended coda signal lasting more than 1 hour after explosion spike (see text). (c) 9.5 hour period of continuous pulsating eruptive activity between 19:59 UTC 9 April and 04:30 UTC 10 April interspersed with eight identifiable individual explosions (see Table 2 for details) and other, lesser perturbations not expressed as clear spikes and therefore of uncertain origin.

Figure 4. Time series of cumulative DRE magma volume with error bounds defining 90% confidence interval of output of stochastic modelling. The last three small explosions of the series are not included in the plot. Two sets of error bounds are shown related to whether K and n are independent or dependent variables and this is discussed in more detail in the text.

Figure 5. Time series of mean erupted DRE magma intensities, by explosion (with $\pm 1\sigma$ uncertainties on mean estimates). The last three small explosions of the series are not included in the plot.

Figure 6. Mean magma discharge rates at times of explosions, by Stage of explosive activity (with $\pm 1\sigma$ uncertainties on mean -- see text). The last three small explosions of the series are not included in the plot.

Figure 7. (a) Repose periods versus time over whole sequence of explosions (including last three small events). (b) Repose period versus time for events up to end of Stage 3.

Figure 8. Reciprocal of repose periods to end of Stage 3. The data suggest a minimum repose period was reached during Stage 1 on 10th April 2021, with repose periods lengthening thereafter.

ACCEPTED MANUSCRIPT

Table Captions

Table 1. Information on explosive events between 9th and 22nd April 2021 at the Soufriere Volcano, St Vincent. All events except 2-4 are short-lived discrete explosions with onset and duration defined by seismic RSAM data. Event 2-4 is period of prolonged continuous but fluctuating explosive activity. The 2-4 tag reflects a legacy numbering system developed in the early stages of the eruption when only three discrete events were identified. The cloud time represents the time of the measurement of cloud height from satellite images. Cloud top temperatures measurements from satellite images with estimates of tropospheric and stratospheric heights for explosive events, except for event 2-4 for which measurements are presented in Table 2. The methods used to estimate the tropospheric and stratospheric heights are presented in the main text. Note heights are above sea level.

Table 2. Explosion events within event 2 of continuous pulsating activity between 1959 UTC (9th April) and 0430 UTC(10th April).

Table 3. Results of stochastic calculations for peak event intensity, event magma volume and accumulative volume with uncertainty statistics.

Table 4. Comparison of DRE volumes (millions of m³) estimated from our study and from analysis of isopach maps (after Cole et al. this volume).

Explosive ID	Day April 2021	OnsetTime (UTC)	Duration (min)	Brightness T ($^{\circ}\text{C}$)	Tropospheric Height (km)	Stratosphere Height (km)	Cloud Time (UTC)
1	9 th	12.36	11	-58	13.0	22.4	12.50
2-4	9/10 th	18.59-04.30	571	Table 3	Table 3		19.10-0430
5	10 th	06.37	11	-40	10.0		0650
6		07.24	3	-66	14.0	20.0	07.50
7		09.35	23	-78	16.0	18.6	09.50
8		10.47	8	-78	16.0	18.6	11.00
9		12.02	12	-78	16.0	18.6	12.10
10		12.54	13	-78	16.0	18.6	13.00
11		14.27	14	-78	16.0	18.6	14.40
12		16.20	23	-78	16.0	18.6	16.30
13		18.50	13	-74	15.2	19.0	18.50
14		21.20	19	-78	16.0	18.6	21.30
15		23.02	20	-80	16.2	18.4	23.10
16	11 th	00.51	21	-80	16.1	17.0	01.00
17		02.44	16	-80	16.1	17.0	02.50
18		04.59	11	-78	15.7	18.7	05.10
19		07.55	13	-72	14.8	19.5	08.10
20		10.36	13	-72	14.9	19.5	10.50
21		13.24	22	-70	14.5	19.9	13.40
22		18.20	11	-64	13.6	20.5	18.20
23		20.22	12	-68	14.0	20.0	20.20
24	12 th	00.39	18	-68	14.0	20.0	00.50
25		07.59	20	-70	14.3	20.0	08.10
26		20.53	24	-52	12.2	25.0	21.30
27	13 th	10.23	24	-68	14.0	19.0	10.40
28	14 th	02.27	17	-64	13.5	20.0	02.40
29		15.31	10	-60	13.0	20.0	15.40
30	16 th	10.16	5		5.2		10.50
31	18 th	20.49	10		5.0		21.00
32	22 nd	15.09	9		5.0		Time uncertain

Table 1

Event ID	Time (UTC)	Duration (min)	Cloud Height
2/1	09/04/2021 18:59	13.0	15.5
2/2	09/04/2021 19:40	2.5	15.5
2/3	09/04/2021 20:29	3.9	14.5
2/4	09/04/2021 22:10	15.8	14.3
2/5	09/04/2021 23:21	7.0	15.7
2/6	10/04/2021 00:11	13.1	15.7
2/7	10/04/2021 00:32	8.6	15.9
2/8	10/04/2021 01:01	9.9	15.9
2/9	10/04/2021 01:43	11.8	15.6
2/10	10/04/2021 02:11	11.8	15.6
2/11	10/04/2021 03:41	12.4	15.3

Table 2

Event	Date time (UTC 2021)	Mean intensity (m ³ /s)	Standard Deviation	5% quantile	50% quantile	95% quantile	Volume (m ³)	Standard Deviation	5% quantile	50% quantile	95% quantile	Acc Vol (m ³)	Standard Deviation	5% quantile	50% quantile	95% quantile
1	(09/04) 12:36	1.63E+03	6.17E+02	8.15E+02	1.53E+03	2.78E+03	4.72E+05	1.79E+05	2.37E+05	4.44E+05	8.06E+05	4.72E+05	1.79E+05	2.37E+05	4.44E+05	8.06E+05
2	(09/04) 18:59	3.44E+03	1.34E+03	1.69E+03	3.22E+03	5.94E+03	1.21E+06	4.74E+05	5.95E+05	1.14E+06	2.09E+06	1.69E+06	6.47E+05	8.36E+05	1.58E+06	2.89E+06
PO1	(09/04) 19:40	3.44E+03	1.34E+03	1.69E+03	3.22E+03	5.94E+03	2.88E+05	1.15E+05	1.39E+05	2.69E+05	5.03E+05	1.97E+06	6.57E+05	1.10E+06	1.87E+06	3.19E+06
PO2	(09/04) 20:29	2.60E+03	1.00E+03	1.29E+03	2.44E+03	4.48E+03	2.61E+05	1.02E+05	1.27E+05	2.44E+05	4.46E+05	2.23E+06	6.65E+05	1.34E+06	2.13E+06	3.46E+06
3	(09/04) 22:10	2.45E+03	9.41E+02	1.21E+03	2.29E+03	4.21E+03	4.73E+05	1.84E+05	2.32E+05	4.43E+05	8.19E+05	2.71E+06	8.39E+05	1.59E+06	2.58E+06	4.27E+06
PO7	(09/04) 23:21	3.63E+03	1.42E+03	1.78E+03	3.40E+03	6.30E+03	7.84E+05	3.02E+05	3.88E+05	7.35E+05	1.35E+06	3.49E+06	8.91E+05	2.26E+06	3.37E+06	5.12E+06
4	(10/04) 00:11	3.63E+03	1.42E+03	1.78E+03	3.40E+03	6.29E+03	1.13E+06	4.43E+05	5.54E+05	1.06E+06	1.96E+06	4.62E+06	1.30E+06	2.86E+06	4.43E+06	7.04E+06
PO9	(10/04) 00:32	3.82E+03	1.50E+03	1.87E+03	3.57E+03	6.63E+03	1.04E+06	4.03E+05	5.08E+05	9.78E+05	1.80E+06	5.67E+06	1.37E+06	3.78E+06	5.49E+06	8.18E+06
PO10	(10/04) 01:01	3.82E+03	1.50E+03	1.87E+03	3.58E+03	6.61E+03	1.09E+06	4.23E+05	5.30E+05	1.01E+06	1.87E+06	6.75E+06	1.43E+06	4.73E+06	6.59E+06	9.35E+06
PO11	(10/04) 01:43	3.53E+03	1.38E+03	1.73E+03	3.30E+03	6.10E+03	6.34E+05	2.51E+05	3.06E+05	5.93E+05	1.11E+06	7.39E+06	1.45E+06	5.32E+06	7.22E+06	1.00E+07
PO12	(10/04) 02:11	3.53E+03	1.38E+03	1.73E+03	3.30E+03	6.12E+03	7.67E+05	3.01E+05	3.72E+05	7.16E+05	1.34E+06	8.15E+06	1.49E+06	6.02E+06	8.00E+06	1.08E+07
PO16	(10/04) 03:41	3.26E+03	1.27E+03	1.60E+03	3.05E+03	5.63E+03	9.08E+05	3.58E+05	4.46E+05	8.47E+05	1.60E+06	9.06E+06	1.53E+06	6.85E+06	8.91E+06	1.18E+07
5	(10/04) 06:37	4.15E+03	1.63E+03	2.03E+03	3.87E+03	7.20E+03	8.29E+05	3.26E+05	4.04E+05	7.75E+05	1.44E+06	9.89E+06	1.81E+06	7.34E+06	9.69E+06	1.32E+07
6	(10/04) 07:24	2.25E+03	8.61E+02	1.12E+03	2.11E+03	3.85E+03	8.76E+04	3.81E+04	3.89E+04	8.07E+04	1.59E+05	9.98E+06	1.84E+06	7.38E+06	9.77E+06	1.33E+07
7	(10/04) 09:35	3.93E+03	1.54E+03	1.93E+03	3.67E+03	6.80E+03	1.78E+06	6.99E+05	8.75E+05	1.67E+06	3.09E+06	1.18E+07	2.46E+06	8.37E+06	1.14E+07	1.63E+07
8	(10/04) 10:47	3.93E+03	1.54E+03	1.92E+03	3.67E+03	6.81E+03	1.11E+06	4.37E+05	5.44E+05	1.04E+06	1.93E+06	1.29E+07	2.87E+06	8.97E+06	1.25E+07	1.82E+07
9	(10/04) 12:02	3.93E+03	1.54E+03	1.92E+03	3.67E+03	6.82E+03	1.02E+06	4.02E+05	5.02E+05	9.58E+05	1.78E+06	1.39E+07	3.25E+06	9.51E+06	1.34E+07	1.99E+07
10	(10/04) 12:54	3.93E+03	1.54E+03	1.92E+03	3.67E+03	6.82E+03	1.32E+06	5.20E+05	6.48E+05	1.24E+06	2.30E+06	1.52E+07	3.74E+06	1.02E+07	1.47E+07	2.22E+07
11	(10/04) 14:27	3.93E+03	1.54E+03	1.92E+03	3.67E+03	6.81E+03	1.15E+06	4.52E+05	5.63E+05	1.08E+06	2.00E+06	1.64E+07	4.18E+06	1.08E+07	1.57E+07	2.42E+07
12	10/04 16:20	3.93E+03	1.54E+03	1.92E+03	3.67E+03	6.81E+03	2.45E+06	9.60E+05	1.20E+06	2.29E+06	4.25E+06	1.88E+07	5.11E+06	1.21E+07	1.80E+07	2.84E+07
13	10/04 18:50	3.17E+03	1.23E+03	1.57E+03	2.97E+03	5.47E+03	7.74E+05	3.03E+05	3.79E+05	7.24E+05	1.35E+06	1.96E+07	5.40E+06	1.24E+07	1.87E+07	2.97E+07
14	10/04 21:20	3.93E+03	1.54E+03	1.92E+03	3.68E+03	6.80E+03	2.25E+06	8.80E+05	1.10E+06	2.10E+06	3.89E+06	2.18E+07	6.25E+06	1.36E+07	2.08E+07	3.36E+07
15	10/04 23:02	4.14E+03	1.62E+03	2.02E+03	3.87E+03	7.17E+03	1.56E+06	6.13E+05	7.62E+05	1.46E+06	2.71E+06	2.34E+07	6.85E+06	1.44E+07	2.23E+07	3.62E+07
16	11/04 00:51	4.03E+03	1.58E+03	1.97E+03	3.77E+03	7.01E+03	1.89E+06	7.40E+05	9.20E+05	1.76E+06	3.28E+06	2.53E+07	7.57E+06	1.53E+07	2.41E+07	3.95E+07
17	11/04 02:44	4.03E+03	1.58E+03	1.97E+03	3.76E+03	7.01E+03	1.76E+06	6.90E+05	8.60E+05	1.64E+06	3.06E+06	2.71E+07	8.25E+06	1.62E+07	2.57E+07	4.25E+07
18	11/04 04:59	3.63E+03	1.42E+03	1.78E+03	3.40E+03	6.30E+03	1.21E+06	4.73E+05	5.93E+05	1.13E+06	2.10E+06	2.83E+07	8.71E+06	1.68E+07	2.68E+07	4.46E+07
19	11/04 07:55	2.83E+03	1.09E+03	1.40E+03	2.65E+03	4.88E+03	1.09E+06	4.23E+05	5.39E+05	1.02E+06	1.88E+06	2.94E+07	9.12E+06	1.74E+07	2.79E+07	4.65E+07
20	11/04 10:36	2.92E+03	1.13E+03	1.44E+03	2.73E+03	5.03E+03	1.42E+06	5.51E+05	6.98E+05	1.33E+06	2.44E+06	3.08E+07	9.66E+06	1.81E+07	2.92E+07	4.89E+07
21	11/04 13:24	2.60E+03	1.00E+03	1.28E+03	2.43E+03	4.48E+03	1.17E+06	4.53E+05	5.80E+05	1.10E+06	2.03E+06	3.19E+07	1.01E+07	1.87E+07	3.03E+07	5.09E+07
22	11/04 18:20	1.98E+03	7.56E+02	9.88E+02	1.86E+03	3.75E+05	1.45E+05	1.85E+05	3.51E+05	6.45E+05	3.75E+05	3.23E+07	1.02E+07	1.89E+07	3.07E+07	5.15E+07
23	11/04 20:22	2.25E+03	8.62E+02	1.11E+03	2.11E+03	5.37E+05	2.06E+05	2.65E+05	5.04E+05	9.23E+05	5.37E+05	3.29E+07	1.04E+07	1.91E+07	3.12E+07	5.24E+07
24	12/04 00:39	2.25E+03	8.62E+02	1.11E+03	2.11E+03	9.24E+05	3.55E+05	4.58E+05	8.67E+05	1.59E+06	9.24E+05	3.38E+07	1.08E+07	1.96E+07	3.20E+07	5.40E+07
25	12/04 07:59	2.45E+03	9.42E+02	1.21E+03	2.29E+03	1.49E+06	5.72E+05	7.35E+05	1.39E+06	2.55E+06	1.49E+06	3.53E+07	1.13E+07	2.03E+07	3.34E+07	5.66E+07
26	12/04 20:53	1.25E+03	4.70E+02	6.29E+02	1.18E+03	6.84E+05	2.57E+05	3.44E+05	6.43E+05	1.16E+06	6.84E+05	3.60E+07	1.16E+07	2.07E+07	3.41E+07	5.77E+07
27	13/04/10:23	2.25E+03	8.63E+02	1.11E+03	2.11E+03	1.22E+06	4.70E+05	6.08E+05	1.15E+06	2.11E+06	1.22E+06	3.72E+07	1.21E+07	2.13E+07	3.52E+07	5.98E+07
28	14/04/02:27	1.92E+03	7.29E+02	9.53E+02	1.80E+03	7.09E+05	2.70E+05	3.52E+05	6.65E+05	1.21E+06	7.09E+05	3.79E+07	1.23E+07	2.17E+07	3.59E+07	6.10E+07
29	14/04/15:31	1.63E+03	6.17E+02	8.17E+02	1.53E+03	5.72E+05	2.17E+05	2.87E+05	5.37E+05	9.75E+05	5.72E+05	3.85E+07	1.25E+07	2.20E+07	3.64E+07	6.20E+07
30	16/04/10:16	2.89E+01	9.71E+00	1.55E+01	2.77E+01	3.93E+03	1.33E+03	2.09E+03	3.76E+03	6.38E+03	3.93E+03	3.85E+07	1.25E+07	2.20E+07	3.64E+07	6.20E+07
31	18/04 20:49	2.48E+01	8.28E+00	1.33E+01	2.37E+01	4.46E+03	1.50E+03	2.39E+03	4.26E+03	7.21E+03	4.46E+03	3.85E+07	1.25E+07	2.20E+07	3.64E+07	6.20E+07
32	22/04 15:09	2.48E+01	8.28E+00	1.33E+01	2.37E+01	5.42E+03	1.82E+03	2.90E+03	5.18E+03	8.78E+03	5.42E+03	3.85E+07	1.25E+07	2.20E+07	3.64E+07	6.20E+07

Table 3

End time of tephra unit	Tephra Unit	Stage	Our result	5 th per	50 th per	95 th perc	Isopach maps	5 th per	50 th per	95 th perc
9/04 0724	U1	1	10.0	7.4	9.8	13.3	13.0	2.8	14.5	30.7
10/04 1830	U2	2	9.6	4.8	9.0	16.6	14.5	7.3	10.3	28.3
10/04 2302	U3	2	3.8	1.9	3.6	6.6	4.7	2.3	3.6	4.7
14/04 1531	U4-7	2* and 3	15.1	7.5	14.1	25.8	7.10	3.1	7.3	10.6

*11/04 0459 end of stage 2.

Table 4



Figure 1

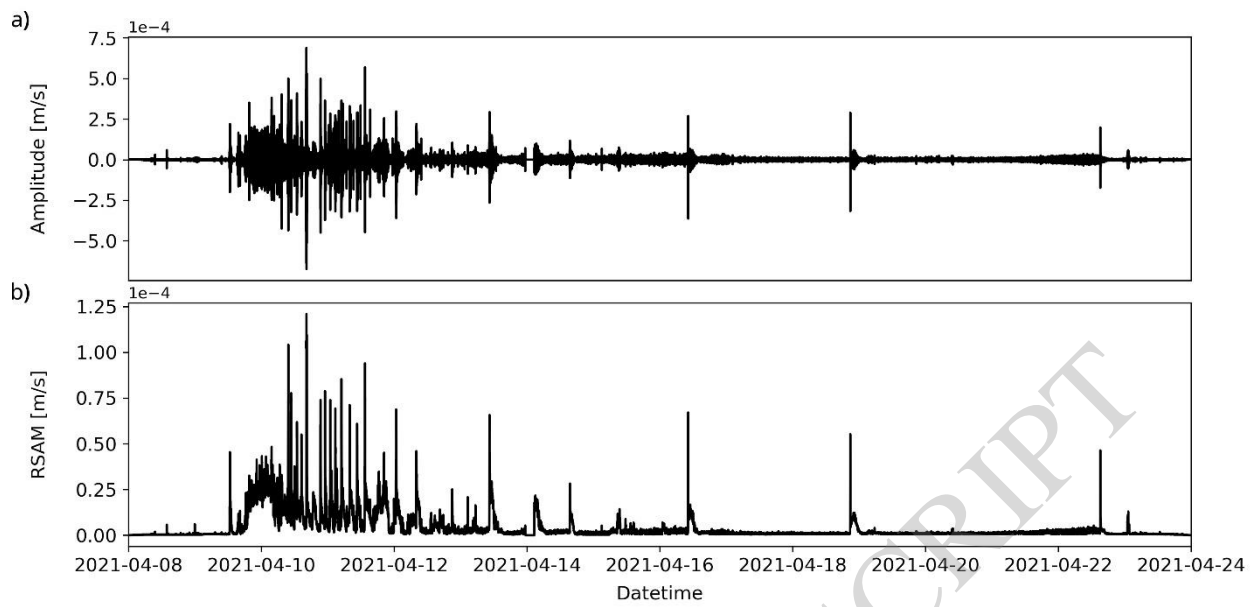


Figure 2

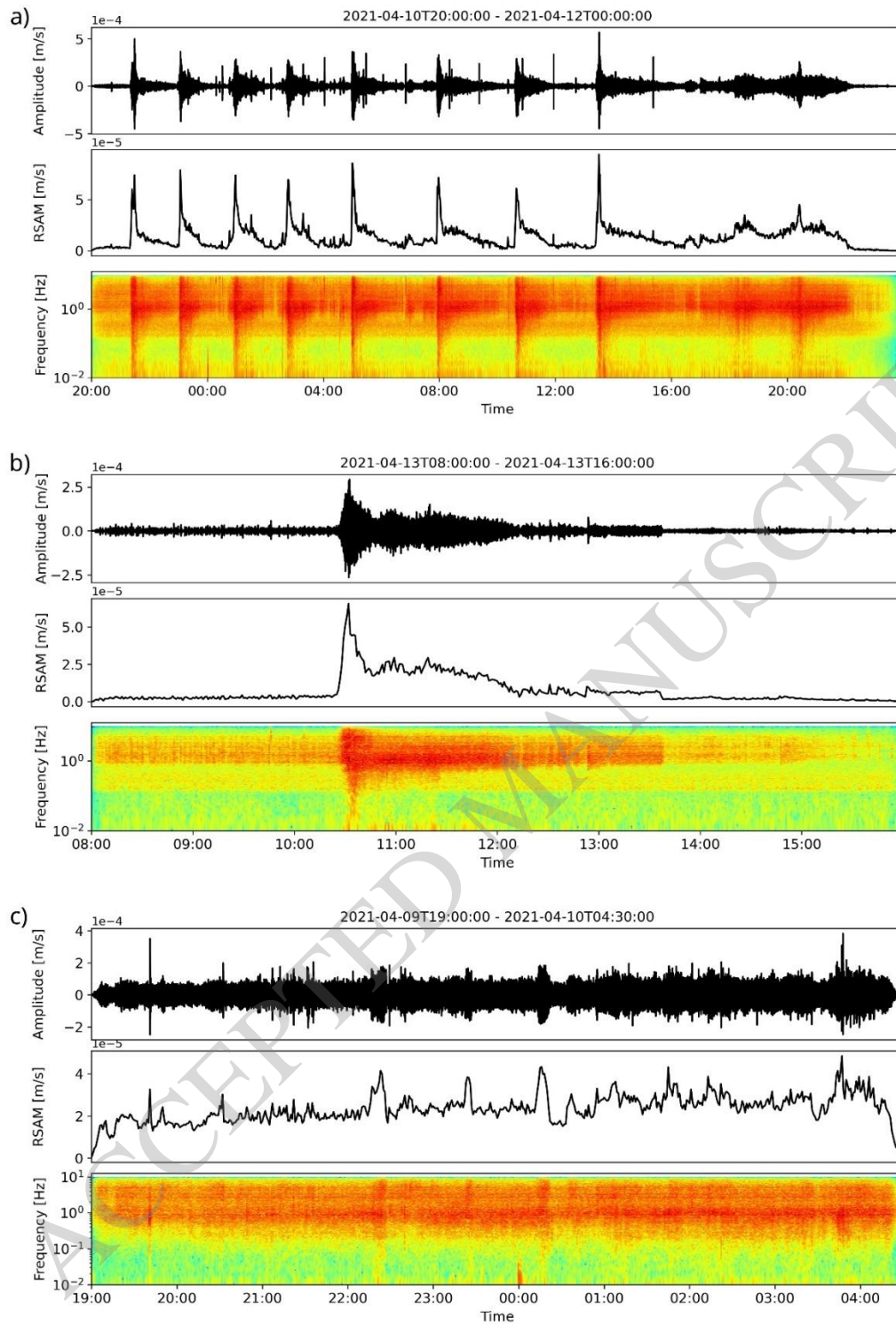


Figure 3

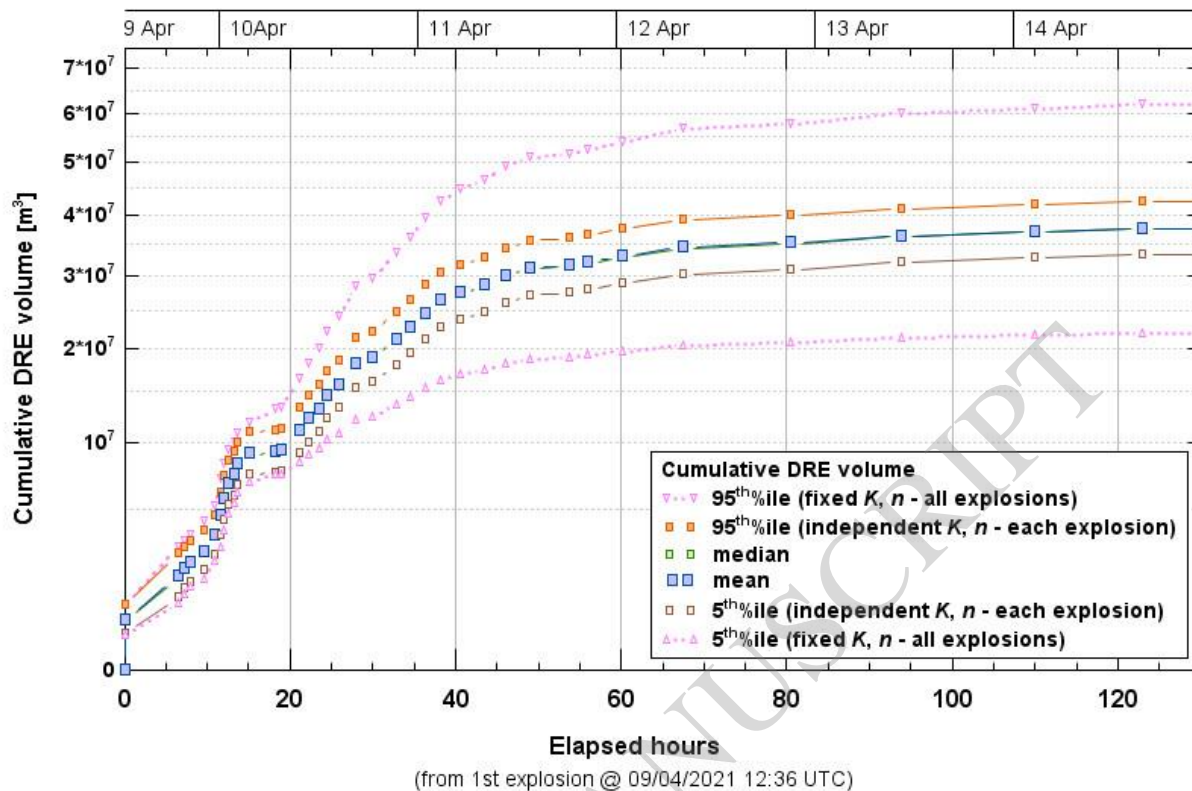


Figure 4

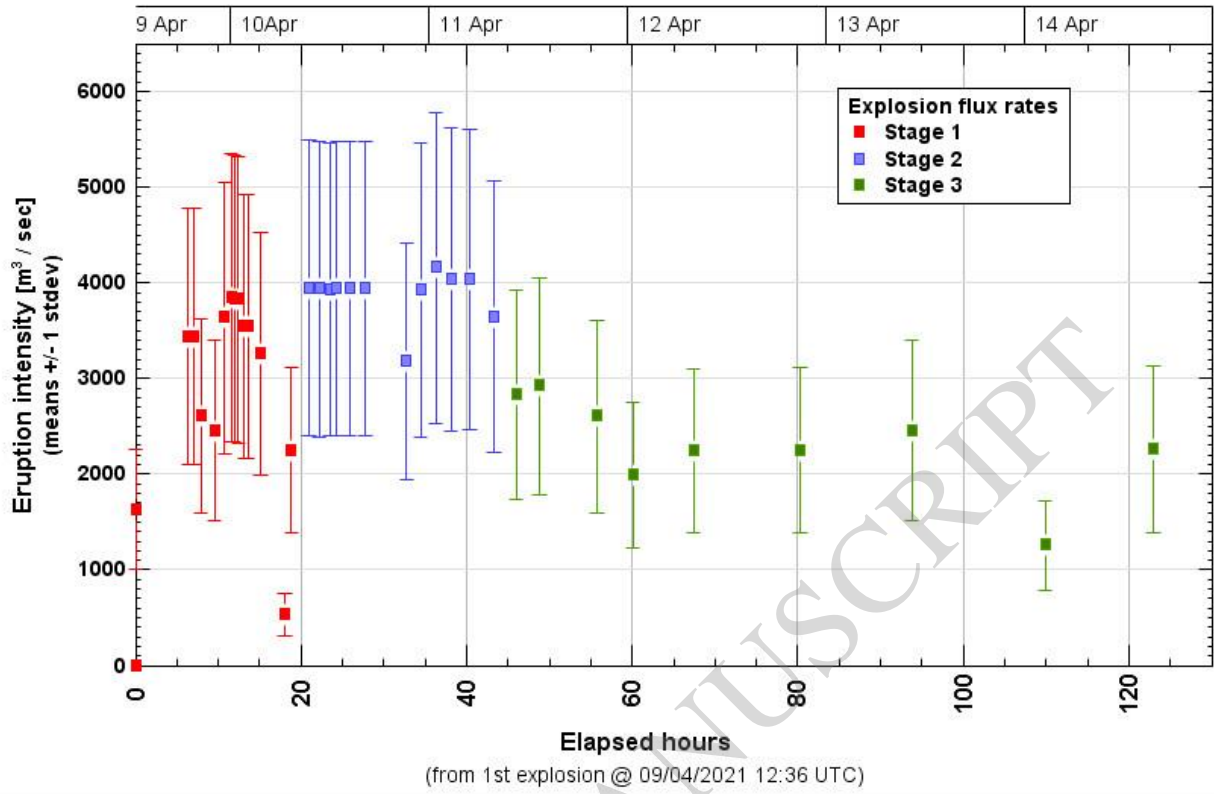


Figure 5

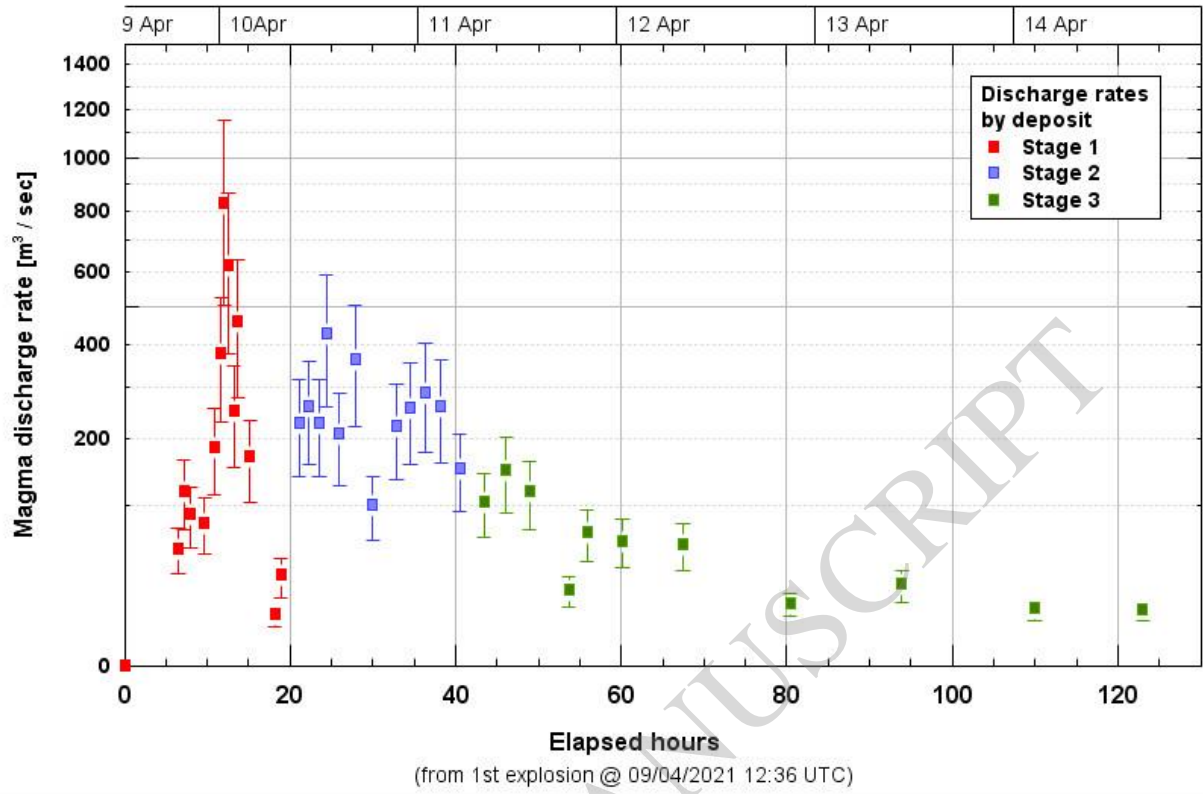


Figure 6

